Journal of Wind Engineering & Industrial Aerodynamics 215 (2021) 104683

Contents lists available at ScienceDirect

Journal of Wind Engineering & Industrial Aerodynamics

journal homepage: www.elsevier.com/locate/jweia

Investigation of the wake propagation behind wind turbines over hilly terrain with different slope gradients

Wei Tian [a,b,*], Kuan Zheng [a], Hui Hu [c]

[a] School of Aeronautics and Astronautics, Shanghai Jiao Tong University, Shanghai, 200240, China
[b] Sichuan Research Institute, Shanghai Jiao Tong University, Chengdu, Sichuan, 610213, China
[c] Department of Aerospace Engineering, Iowa State University, Ames, IA, 50010, USA

ARTICLE INFO

Keywords:
Wind energy
Wind turbine
Complex terrain
Wake characteristics
Actuator disk

ABSTRACT

In this study, a Reynolds-averaged Navier-Stokes (RANS) numerical simulation with wind turbine simulated through actuator disk model was conducted to quantify the characteristics of wind turbine wake over two-dimensional Gaussian hills with different slope gradients. The simulated flow characteristics in the wind turbine wake, such as velocity deficit, wake expansion and wake centerline, were compared with those given by the Jensen wake model to quantitatively evaluate the accuracy of the current engineering wake model for the optimal design of wind turbine layout over complex terrain. For the gentle slope hill, the topography behind the wind turbine has a significant effect on the wake characteristics, which is not taken into account in the Jensen wake model. A new method for calculating wake velocity is proposed based on the local speed-up factor and the simulated velocity in the wake of wind turbine sited on flat terrain that can more reasonably predict the wake velocity over complex terrain. For the steep slope hill, the propagation of wind turbine wake is not related to the hill shape in the region behind the hilltop. The assumption that the wake centerline follows the surface of the hill in the Jensen wake model is no longer applicable. The recovery of wind turbine wake in the far wake region was always faster for the steep slope hill compared with the gentle slope hill case. This acceleration of wake recovery is thought to be closely related to the separation flow at the lee side of the hill, which highly restricts the downward deflection and expansion of the wind turbine wake.

1. Introduction

Wind energy, one of the cleanest renewable energy resources, has developed rapidly over the past two decades. Given that numerous suitable sites on flat terrain have been established, the exploration of complex terrains appropriate for wind farm installation is critically important for ensuring the growth of wind energy capacity and has thus received increased attention. Compared with flat terrain, wind turbines sited over complex terrain could generate higher power because of the speed-up effect. However, complex terrains also have negative effects on wind turbine performance because of the more complex flow conditions (i.e., enhanced turbulence level, high wind shear and flow separation). Therefore, it is crucial for the wind farm layout design on complex terrain to leverage the speed-up effects for maximizing energy production, and meanwhile minimizing the negative effects caused by the complex flow conditions.

In wind farms, the wake interference of upstream turbines leads to lower power outputs and higher fatigue loads of the downstream wind turbines. Compared with wind turbines experiencing freestream conditions, downstream wind turbines may experience losses in power up to 30% (Barthelmie et al., 2007; Chu and Chiang, 2014; El-Asha et al., 2017) and fatigue loads as high as 80% (Thomsen and Soerensen, 1999). The wake interference between wind turbine arrays is considered a key research topic in the field of wind energy (Schreck et al., 2008). Numerous field tests (Garcia et al., 2018; Zhan et al., 2020), experimental (Hu et al., 2012; Tian et al., 2014) and numerical (Shayan et al., 2018; Behrouzifar and Darbandi, 2019) studies have been performed to characterize the turbulent wake flows and wake interference between wind turbines. Based on these studies, different wake models (Barthelmie et al., 2006; Tian et al., 2015; Göçmen et al., 2016; Cheng and Fernando, 2018; Ge et al., 2019a, 2019b; Keane, 2021) have been developed and incorporated into commercial software for wind farm layout design.

However, for wind farms on complex terrain, complex flow conditions over different terrain features significantly affect the evolution of

* Corresponding author. School of Aeronautics and Astronautics, Shanghai Jiao Tong University, Shanghai, 200240, China.
E-mail address: tianwei@sjtu.edu.cn (W. Tian).

https://doi.org/10.1016/j.jweia.2021.104683
Received 17 January 2021; Received in revised form 12 May 2021; Accepted 29 May 2021
Available online 20 June 2021

Nomenclature

C_L	Lift coefficient
C_D	Drag coefficient
C_T	Thrust coefficient of the wind turbine
D	Rotor diameter of the wind turbine
D_w	Wake zone diameter
H	Hub height
L	Length between the hill height form $h/2$ to h
Re_c	Reynolds number based on the chord length
S	Speed-up factor
U_H	Incoming wind speed at hug height over flat terrain
U_{rel}	Relative velocity to the airfoil element
U_x	Axial velocity
U_θ	Tangential velocity
Ω	Turbine angular velocity
$\Delta U/U_H$	Normalized velocity deficit
c	Chord length
h	Height of the hilltop
l	Downstream curved distance for upstream wind turbine
q	Wake expansion coefficient
r	Radius of the blade element
s	Hill slope
u*	Friction velocity
z_0	Surface roughness length
α	Angle of attack
β	Pitch angle
ϕ	Angle between U_{rel} and the rotor plane
ρ	Air density

Subscript

WT	Condition with wind turbine
0	Condition without wind turbine

wind turbine wake. Therefore, the characteristics of wind turbine wake are highly dependent on topography. Hansen et al. (2016) analyzed the wind turbine wake properties in complex terrain based on the supervisory control and data acquisition (SCADA) data from a field test of wind farm. Menke et al. (2018) analyzed the wake of a single wind turbine in complex terrain by using measurements from lidars. The results show a strong dependence of the vertical wake propagation on the atmospheric stability. Lange et al. (2017) investigated flow field over a large-scale model of the Bolund peninsula in a wind testing chamber. They found that the mean wind, wind shear and turbulence level are extremely sensitive to the exact details of the terrain. The minor changes in the terrain affect not only the power performance but also the life-time and maintenance costs of wind turbines. In addition, a wind tunnel test was conducted by Hyvärinen et al. (2018) to study the wake development over sinusoidal hills with wind turbines placed on the ridges of the hills. Besides field tests and wind tunnel measurements, a number of numerical simulations were also conducted to investigate the wind turbine wake characteristics over complex terrain. Politis et al. (2012) conducted a computational fluid dynamics (CFD) simulation to investigate the effect of terrain on wake development for a wind turbine sited on the top of an axisymmetric and a quasi-three dimensional Gaussian hill. They found that the hill terrain affects the evolution of the wind turbine wake in a complicated manner. Yang et al. (2015) simulated the wake characteristics of wind turbine sited downstream of a three-dimensional hill using large-eddy simulation (LES) with an actuator line model. The simulation results were consistent with the experimental measurements made by Howard et al. (2015). Shamsoddin and Porté-Agel (2018) presented an analytical modeling framework together with LES results to investigate turbine wakes over two-dimensional hills. In addition to the simplified hill models, numerical simulations were also performed to evaluate the wind turbine wakes in realistic complex terrains. Makridis and Chick (2013) used a combined Reynolds-averaged Navier-Stokes (RANS)/actuator disk method to simulate the wind turbine wakes in Askervein Hill and Bahia. Nedjari et al. (2017) simulated the wake flow of wind turbine sited over complex terrain with a method combining CFD with the actuator disk model. Berg et al. (2017) presented LES results of a turbine wake in realistic complex terrain with slopes above 0.5 (double ridge Perdigao in Portugal). Astolfi et al. (2018) simulated a cluster of four 2.3 MW wind turbines sited in a complex terrain using a steady-state RANS CFD model. In their research, a novel way of elaborating the simulation results was proposed and confirmed by SCADA data analysis. Recently, Shen et al. (2019) simulated the flow over a complex terrain located in China and computed the wind farm power with a RANS/actuator disk CFD method.

Although CFD simulations can provide detailed information on the wind turbine wake for various complex terrains, the computational costs are high, limiting their use in wind farm layout design. There is thus a need to develop accurate wake models for complex terrain to reduce computational costs. Few studies have modeled the wind turbine wake effects on complex terrain. Song et al. (2012) developed a virtual particle tracking model to compute the characteristics of wind turbine wake over complex terrain. Feng and Shen (2014) utilized an adapted Jensen wake model to evaluate the wake effects using the inflow conditions of complex terrain as inputs. Kuo et al. (2016) proposed a novel wake model to reduce computational costs by solving a simplified variation of the Navier-Stokes equations. In addition, an engineering wake model considering acceleration on a two-dimensional hill was developed by Ibrahim et al. (2019) based on the momentum theory.

The wake characteristics for the wake models used for complex terrain are generally obtained by a two-step decoupled approach. The first step is to calculate the flow field over complex terrain without the installation of wind turbines. Flow characteristics such as speed-up factors, wind direction and turbulence levels can be obtained from the calculated flow field. In the second step, the change in flow characteristics (e.g., velocity deficit, wake expansion, wind turning and enhanced turbulence) caused by the installation of wind turbines can be calculated based on the traditional wake model developed for flat terrain and the flow characteristics over complex terrain obtained in the first step. The wake models mentioned above can significantly reduce computational costs compared with the full CFD simulation.

The Jensen wake model is an engineering wake model that is widely used in commercial software (e.g., WindSim, WindPro, OpenWind) (Jensen, 1983). The wind speed in the wind turbine wake over complex terrain can be obtained by combining the original Jensen wake model and the speed-up factors:

$$u(l) = U_H S\left[1 - \frac{1-\sqrt{1-C_T}}{(1+2ql/D)^2}\right] \tag{1}$$

where S is the speed-up factor of the wind turbine location at the hub height level, l is the downstream curved distance from the wind turbine, U_H is the reference wind speed (i.e., incoming wind speed at hub height over flat terrain), C_T is the thrust coefficient of the wind turbine, D is the rotor diameter, and q is the wake expansion coefficient. q can be calculated by the following empirical formula (Frandsen, 1992):

$$q = \frac{0.5}{ln(H/z_0)} \tag{2}$$

where z_0 and H are the surface roughness length and the turbine hub height, respectively.

The wake zone diameter can also be determined by the Jensen wake model:

$$D_w(l) = D + 2ql \tag{3}$$

In this study, a RANS simulation combined with actuator disk model was applied to obtain the wake characteristics over two-dimensional Gaussian hills with both gentle and steep slope. Although previous studies have primarily focused on wind turbines sited on hilltops such that the wind turbines benefit from the richest wind resource, the wind turbines cannot always be installed on hilltops because of the limitations relating to land use and installation costs. In this study, a more comprehensive simulation is performed with wind turbines installed at different locations over hilly terrain with both gentle and steep slopes. The remainder of this paper is organized as follows. In section 2, the actuator disk method is first introduced. The computational domain, boundary conditions and case validation can be seen later in this section. Numerical results are presented and discussed in Section 3. The simulated flow characteristics in the wind turbine wake, such as velocity deficit, wake expansion and wake center, are systemically analyzed and compared with those generated by the Jensen wake model. In addition, a new method for calculating wake velocity is proposed in this section for the optimal design of the wind turbine layout over complex terrain. Section 4 briefly concludes this simulation work.

2. Numerical methodology

In this study, a three-dimensional and steady-state numerical computation was conducted to simulate the wake characteristics of wind turbine sited over complex terrain. The incompressible RANS equations were solved with a commercial software (ANSYS Fluent 16.5). The pressure-based solver was selected given that it is generally used for incompressible flow. Turbulence closure was achieved using the RNG $k-\varepsilon$ model, which is suitable for the prediction of flow over complex terrain with regions of flow separation (Kim et al., 2000). The accuracy of the computation has been validated by Makridis and Chick (2013) and Blocken et al. (2007). The second-order upwind scheme was used for the spatial discretization of momentum, and the first-order upwind scheme was used for the interpolation of turbulent kinetic energy k and turbulent dissipation rate ε. The face pressure was solved using the second-order scheme. The SIMPLE algorithm was used to establish the pressure and velocity coupling.

2.1. Actuator disk method

In the present study, instead of directly simulating the wind turbine, an actuator disk method was introduced to simulate the evolution of wind turbine wake over complex terrain. In this approach, wind turbine rotor is modeled as a momentum sink based on the actuator disc approach and blade element theory (BET). By adding source terms in momentum equations through user-defined functions, the simulations of turbine wake can be highly simplified without meshing the turbine blades. Compared with the uniformly loaded disk model developed from one-dimensional momentum theory (Prospathopoulos et al., 2008), the actuator disk method used in this study considers the change in wind loads in the spanwise direction, which more closely resembles the behavior of wind loads acting on real wind turbine blades.

According to BET, the turbine blade is divided into a finite number of blade elements that are assumed to aerodynamically behave as 2D airfoils, as shown in Fig. 1. The geometric and aerodynamic properties are assumed to be the same for each blade element. The aerodynamic force acting on the blade element can be calculated using the lift and drag coefficients of the airfoil under the local flow conditions.

Fig. 2 shows the schematic of aerodynamic force and velocity vectors relative to the cross-section of a blade element at radius r. The axial and tangential velocities are defined as U_x and U_θ, respectively. The local velocity relative to the rotating blade can be given as:

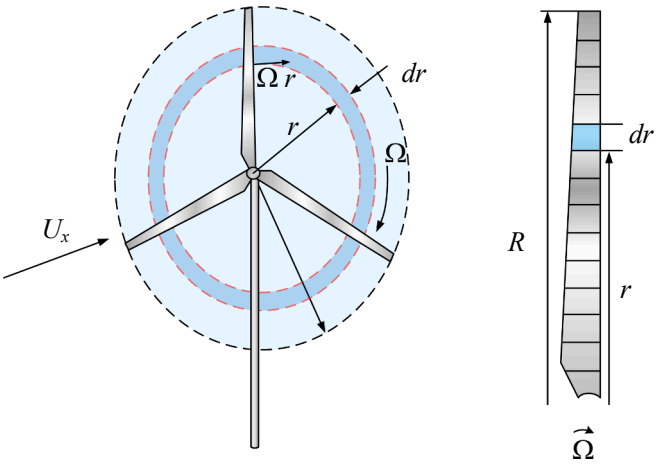

Fig. 1. Schematic of the rotating element, where dr is the spanwise length of the blade element, and Ω is the rotor rotational speed.

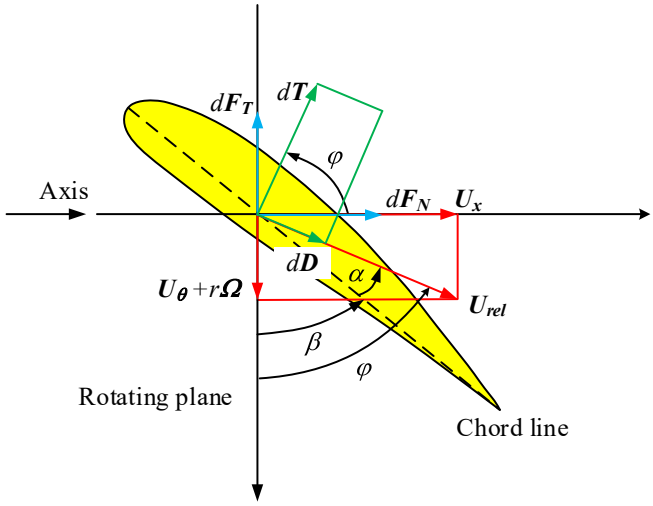

Fig. 2. Schematic of the cross-sectional blade element.

$$\boldsymbol{U_{rel}} = (U_x, U_\theta + \Omega r) \tag{4}$$

The axial and tangential velocities can be calculated as follows:

$$U_x = U_\infty(1-a) \tag{5}$$

$$U_\theta = \Omega r a' \tag{6}$$

where U_∞ is the undisturbed freestream axial velocity, and a and a' are the induction factors in the axial and tangential directions, respectively. The induction factors can be solved using blade element momentum (BEM) theory through numerical iteration.

The angle of attack is defined as:

$$\alpha = \phi - \beta \tag{7}$$

where $\phi = \tan^{-1}(U_x/(U_\theta + \Omega r))$ is the angle between U_{rel} and the rotor plane, and β is the local pitch angle.

The force acting on the blade element is calculated as:

$$\boldsymbol{F} = \frac{\rho U_{rel}^2 c}{2} dr(C_L \boldsymbol{e_L} + C_D \boldsymbol{e_D}) \tag{8}$$

where ρ is the air density; $C_L = C_L(\alpha,\ Re_c)$ and $C_D = C_D(\alpha,\ Re_c)$ are the lift and drag coefficients of the airfoil, respectively; Re_c is the Reynolds number based on the relative velocity U_{rel} and the chord length c; and $\boldsymbol{e_L}$

and $\boldsymbol{e_D}$ are the direction of the unit vector for the lift and drag forces, respectively.

Considering an annular volume of the differential size, $dV = dAdx$, the body force acting on per unit volume is calculated as:

$$\boldsymbol{f} = \frac{d\boldsymbol{F}}{dV} = \frac{d\boldsymbol{F}}{dAdx} = \frac{\rho U_{rel}^2 c}{4\pi r \cdot dx} N_B (C_L \boldsymbol{e_L} + C_D \boldsymbol{e_D}) \tag{9}$$

where $dA = 2\pi r dr$, and N_B is the number of turbine blades.

As indicated by Wu and Porté-Agel (2011), the parameterized forces, which are treated as a source term, need to be distributed smoothly to avoid singular behavior and numerical instability. Following the method proposed by Mikkelsen (2004), the parameterized forces are distributed smoothly in a one-dimensional Gaussian manner. The force $\boldsymbol{f_\varepsilon}$ is formed by taking the convolution of the local load, $\boldsymbol{f}$, and a regularization kernel, η_ε.

$$\boldsymbol{f_\varepsilon} = \boldsymbol{f} \otimes \eta_\varepsilon \tag{10}$$

where

$$\eta_\varepsilon = \frac{1}{\varepsilon \pi^{\frac{1}{2}}} e^{-\left(\frac{d}{\varepsilon}\right)^2} \tag{11}$$

where ε is a constant that adjusts the strength of the regulation function, and d is the streamwise distance between the grid points and the blade element.

2.2. Computational domain

The computational layout and coordinate system are shown in Fig. 3. The origin of the coordinate system is placed at the center of the hill. The longitudinal, transverse and vertical direction are denoted by x, y and z, respectively. An auxiliary vertical coordinate z' was used to represent the height above the hill surface. The height of the computational domain is $L_z = 2.3\,m$, which is consistent with the wind tunnel height reported by Tian et al. (2018). The length and width of the computational domain are set to be $L_x = 71.4\,D$ and $L_y = 8.6\,D$, respectively, where D is the diameter of the wind turbine rotor.

In this study, two typical two-dimensional Gaussian hills with different slopes were simulated. The Gaussian hill shape is defined as:

$$z = h * \exp\left[-\left(\frac{x}{L}\right)^2 \ln 2 \right] \tag{12}$$

where h is the height of the hilltop, L is the length between the hill height from $h/2$ to h. The hill slope is defined as $s = (h/2)/L$. Two hill models with the slope of $s = 0.25$ and $s = 1.0$ were simulated in this study. Several typical positions were selected for the wind turbine siting. For the gentle slope hill (i.e., $s = 0.25$), the selected positions are $6D$ and L in front of the hilltop and on the hilltop, and L and $6D$ downstream of the hilltop (i.e., $x_{WT} = -6D, -L, 0, L, 6D$). For the steep slope hill (i.e., $s = 1.0$), the two positions behind the hilltop (i.e., $x_{WT} = L, 6D$) are not studied because of the occurrence of flow separation in that region, which makes it unsuitable for the installation of wind turbines.

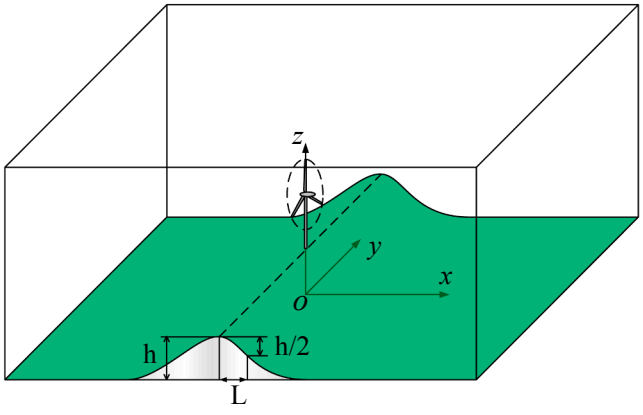

Fig. 3. Computational domain and coordinate system.

2.3. Atmospheric boundary layer (ABL) conditions

The mean streamwise velocity profile of the ABL wind used in this study is determined using a logarithmic function, which can be described as:

$$U(z) = \frac{u_*}{\kappa} ln\left(\frac{z + z_0}{z_0}\right) \tag{13}$$

where $\kappa \approx 0.4$ is the von Karman constant, u_* is the friction velocity, and z_0 is the roughness length.

Instead of simply using a constant inflow turbulence kinetic energy (TKE), the TKE simulated in this study was set to vary with height, which is consistent with the TKE behavior of real ABL wind. The TKE k is expressed as:

$$k = \frac{u_*^2}{\sqrt{C_\mu}} \sqrt{C_1 \cdot ln\left(\frac{z + z_0}{z_0}\right) + C_2} \tag{14}$$

where C_1 and C_2 are constants, and their values are determined by the TKE profile measured in the wind tunnel experiments; C_μ is a constant of the $k - \varepsilon$ turbulence model. For the modeling of neutral equilibrium ABL wind, the value of C_μ is commonly suggested to be $C_\mu = u_*^4/k^2$. In this study, the value of C_μ is set to 0.09.

According to the study of Yang et al. (2009), the turbulence dissipation rate ε applied in the RNG $k - \varepsilon$ model is determined as:

$$\varepsilon = \frac{u_*^3}{k(z + z_0)} \sqrt{C_1 \cdot ln\left(\frac{z + z_0}{z_0}\right) + C_2} \tag{15}$$

Based on the experimental data reported by Tian et al. (2018), the fitted constants shown in Eqn. 13–15 are $u_* = 0.30\,m/s$, $z_0 = 0.30\,mm$, $C_1 = 0.29$ and $C_2 = 1.04$. The comparison of inflow conditions between this study and the experimental study is shown in Fig. 4. The velocity and TKE data shown in Fig. 4 are all normalized by U_H, which is the inflow wind speed at the turbine hub height. The mean velocity and TKE profiles simulated in the present study are consistent with the experimental results.

The two sides and the top surfaces of the computational domain are all set to be symmetry boundaries, which means that the velocity vectors on these surfaces are parallel to the wall. The ground of the computational domain is modeled as a rough wall with a standard wall function (Blocken et al., 2007). The roughness height on the ground is linked with the aerodynamic roughness length z_0 by the following formula:

$$K_s = \frac{E z_0}{C_s} \tag{16}$$

where C_s is a roughness constant, and E is an empirical constant. In this study, the values of C_s and E are set to 0.75 and 9.80, respectively.

2.4. Validation

As mentioned above, the computational domain and the inflow conditions were simulated according to the wind tunnel study performed by Tian et al. (2018). Therefore, the corresponding experimental results were used to validate the accuracy of the current numerical simulation. Fig. 5 shows a comparison of the mean velocity profiles between the experiments and the simulation results for selected locations over the hilly terrain ($x = -3D, 0, 3D, 6D$). From Fig. 5, it can be

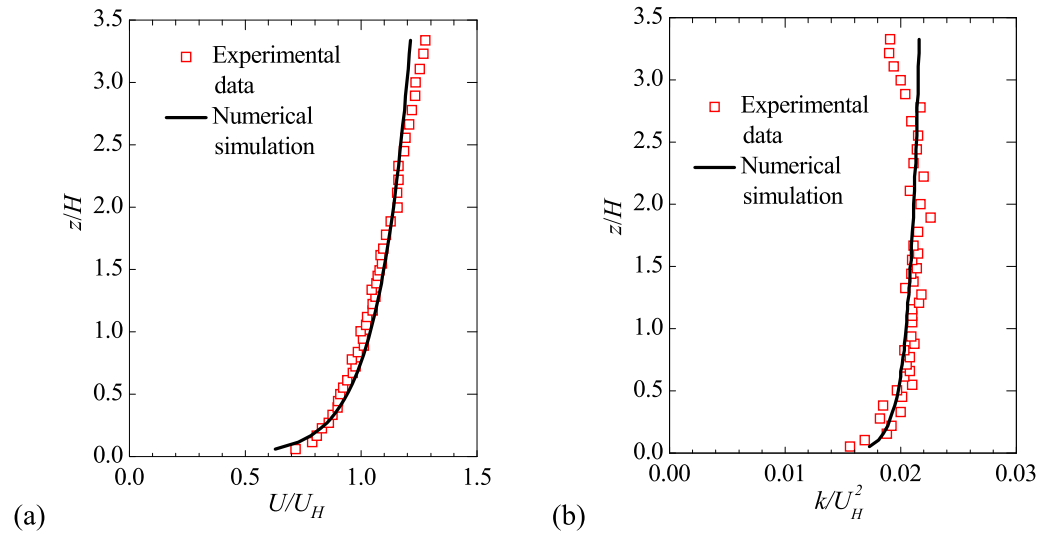

Fig. 4. Comparison of incoming ABL wind characteristics between the present simulation and the experiments data (Tian et al., 2018). (a) velocity profile; (b) turbulent kinetic energy profile.

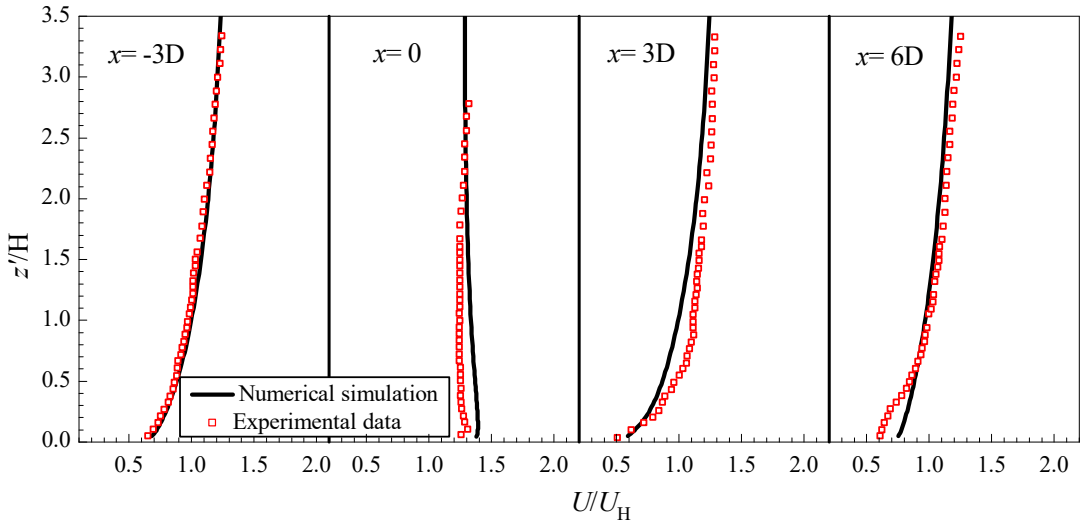

Fig. 5. Comparison of the simulated and the measured mean velocity profiles at different locations over the hilly terrain with the slope of.$s = 0.25$

found that the present simulation results are in good agreement with the experimental data at different locations over the hilly terrain. The present simulation is able to accurately capture the speed-up effect at the windward side of the hill, as well as the subsequent decrease of wind speed in the region behind the hilltop.

The velocity profiles obtained 6D downstream of the wind turbine sited on the hilltop are plotted in Fig. 6 to evaluate the accuracy of the wind turbine wake simulation. The maximum difference in the velocities between the experimental (Tian et al., 2018) and the simulation results was approximately 5%, which is acceptable for the prediction of wind turbine wake characteristics over complex terrain.

3. Results and discussion

3.1. Gentle slope hilly terrain

The velocity deficit contours caused by the wake flow of wind turbine sited at different positions over the gentle slope hill are plotted in Fig. 7. The normalized velocity deficit shown in Fig. 7 is defined as follows:

$$\frac{\Delta U}{U_H} = \frac{U_0 - U_{WT}}{U_H} \tag{17}$$

where U_{WT} and U_0 are the flow velocity over hilly terrain with and without wind turbine installed, and U_H is the inflow wind speed at turbine hub height on flat terrain.

The effect of topography on the evaluation of wind turbine wake can be clearly observed in Fig. 7. As shown in Fig. 7(a), for the wind turbine located at the position of $x_{WT} = -6D$, the velocity deficit profiles in the near-wake region do not differ from that of the flat terrain case. However, in the far wake region, the velocity deficit decreases more rapidly in the hilly terrain case. This difference is associated with the speed-up effect at the windward side of the hill, which accelerates the recovery of the wind turbine wake. In addition, the wake expansion at the windward side of the hill is highly restricted because of the increase in hill height.

For the wind turbine placed at $x_{WT} = -L$, the speed-up effect over the windward side of the hill greatly accelerates the recovery of wind turbine wake in the near wake region. As shown in Fig. 7(b) and (f), the size of the region with high velocity deficit (i.e., $\Delta U/U_H > 0.1$) became much smaller relative to that observed in the flat terrain case. The

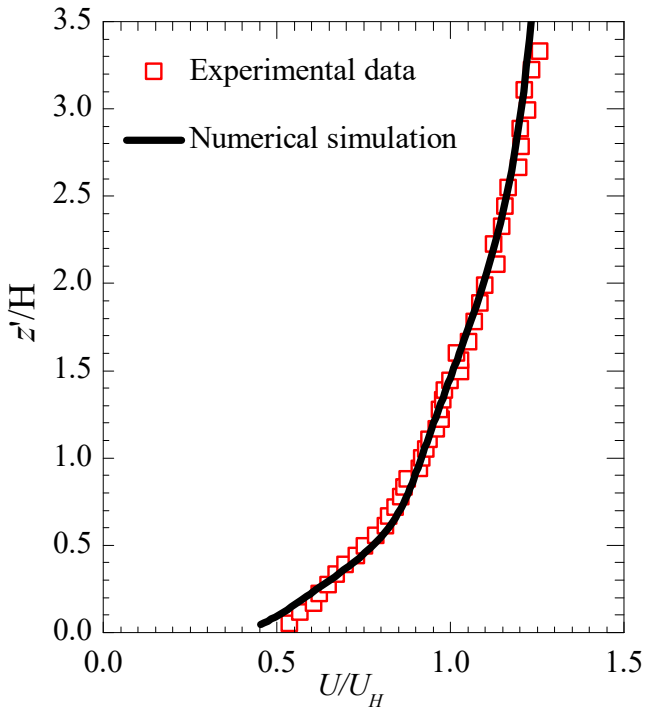

Fig. 6. The velocity profiles obtained 6D downstream of the wind turbine sited on the hilltop.

restriction on wake expansion can also be observed in the region at the windward side of the hill. In the region behind the hilltop, the recovery of wind turbine wake was found to slow down gradually.

As shown in Fig. 7(c), the wake flow of wind turbine sited on the hilltop shows much higher velocity deficits in both the near and far wake region than in the flat terrain case. The size of the region with high velocity deficit (i.e., $\Delta U/U_H > 0.1$) can extend to $6D$ downstream of the wind turbine, which is approximately 1.5 times that of the flat terrain case. These changes in wake characteristics indicate that the wake effect can be significantly enhanced by the topography with flow moving over the lee side of the hill. This enhanced wake effect can be attributed to the adverse pressure gradient over the lee side of the hill, which resists the movement of fluid particles and restricts the turbulent mixing in the wind turbine wake region. For cases in which the wind turbine is located in front of the hilltop ($x_{WT} = -6D, -L$), the slowdown of wake recovery at the lee side of the hill is also caused by the adverse pressure gradient in this region. Compared with the flat terrain case, the wake flow can expand to a much wider range in the vertical direction at the lee side of the hill because of the decrease in hill height. The wake behavior for the wind turbine sited at the downgrade of the hill ($x_{WT} = L$) was found to be similar to that of the case in which the wind turbine is sited on the hilltop. It can be seen in Fig. 7(d) that the velocity deficit in the wind turbine wake is always higher than that of the flat terrain case.

With wind turbine moving to $6D$ downstream of the hilltop ($x_{WT} = 6D$), the effect of topography on the wake characteristics becomes much weaker compared with the previously discussed wind turbine locations. Only a slight downwash of the wake flow can be observed in Fig. 7(e). In addition, a small decrease in the velocity deficit can be obtained compared with the flat terrain case, which is mainly caused by the enhanced turbulent kinetic energy induced by the upstream hill.

Fig. 8 shows the centerline of the wake zone with wind turbine sited at different locations of the hilly terrain. Here, the wind turbine wake center is defined as the point corresponding to the maximum velocity deficit. The propagation of wind turbine wake is highly dependent on the topography. If the hill height changes sharply, the centerline of wind turbine wake has an obvious delay compared with the change in hill height, which can be observed clearly in the near wake region of wind turbine located on the windward side of the hill ($x_{WT} = -L$) and on the hilltop ($x_{WT} = 0$). With wake flow moving further downstream, the wake centerlines gradually adjust to follow the terrain curvature along the wind direction in the far wake region. For the wind turbine sited at the location of $x_{WT} = L$, the change in hill height has greatly slowed down in the region downstream of the wind turbine. Therefore, it can be seen in Fig. 9(d) that the centerline of the wind turbine wake can accurately follow the terrain shape in both the near and far wake region.

The wake models adopted in commercial software typically assume that the centerline of the wind turbine wake follows the terrain curvature along the wind direction with the wake center height equal to the wind turbine hub height H. As shown in Fig. 8, this assumption is reasonable for cases with wind turbines located at $x_{WT} = -L$ and L, especially for wind turbine wake in the region behind $x = L$. For the wind turbine sited on hilltop ($x_{WT} = 0$), the decline in the wake center does not follow the sharp decrease in hill height in the region between $x = 0$ and $x = L$. The wake center height at the location of $x = L$ is $1.3H$. After the location of $x = L$, the wake center can reasonably follow the hill shape with the height of approximately $1.3H$. Therefore, it can be seen in Fig. 8 that the wake center is always higher than the wind turbine hub height H.

For the wind turbine sited in front of the hill ($x_{WT} = -6D$), the wake center height cannot increase as rapidly as hill height over the windward side of the hill, which makes the wake center gradually move towards the hill surface. It can be seen in Fig. 8 that the height of the wake center on the hilltop decreased to approximately $H/3$. With further development of the wake flow, the height of the wake center gradually changes to $H/2$ at the location of $x = 4D$ and then follows the terrain shape with a relatively constant wake center height (i.e. $H/2$). Therefore, the assumption used in commercial software is not applicable to wind turbines sited in front of the hill because the height of the wake center over the hill is much lower than the wind turbine hub height H.

Fig. 9 shows the hub height velocity deficit profiles for wind turbines sited at different locations over the hilly terrain. The profile corresponding to the flat terrain case is also plotted for comparison. The abscissa axis in Fig. 9 is l/D, where l is the downstream curved distance away from the wind turbine. For the wind turbines located at $x_{WT} = -6D$ and $-L$, the recovery of wind turbine wake in front of the hilltop is much faster than in the flat terrain case. After the hilltop, the velocity deficits first increase to the same level as that of the flat terrain case and then decrease gradually with the further development of the wind turbine wake. Therefore, there are two turning points in the velocity deficit profiles. The first turning point is at the hilltop, and the distance between the first and the second turning points is found to be nearly the same as the distance between the wind turbine and the hilltop, as shown in Fig. 9(a) and (b). Second, a dramatic increase in the velocity deficit can be observed in the wake region for the wind turbine sited on the hilltop and at the downgrade of the hill ($x_{WT} = 0$ and L). It can be seen in Fig. 9(c) and (d) that the difference in the velocity deficits between the hilly terrain and the flat terrain cases can last a long distance downstream of the wind turbine. Third, because of the enhanced turbulent kinetic energy caused by the upstream hill, a decrease in the velocity deficit can be observed in Fig. 9(e) for the wind turbine sited behind the hill relative to that of the flat terrain case.

The simulation results described above indicate that applying the Jensen wake model to predict wake characteristics over hilly terrain would result in obvious errors. As shown in Eqn. (1), only the speed-up factor at the wind turbine location is adopted in the Jensen wake model. The effect of downstream topography on the wind turbine wake is not taken into consideration. As shown in Fig. 10(a) and (b), for the wind turbine sited in front of the hilltop, the wind turbine wake is significantly affected by the downstream topography, which obviously cannot be reflected by the Jensen wake model.

In this study, we proposed another way to predict the hub height velocity distribution in the wind turbine wake, which can be calculated

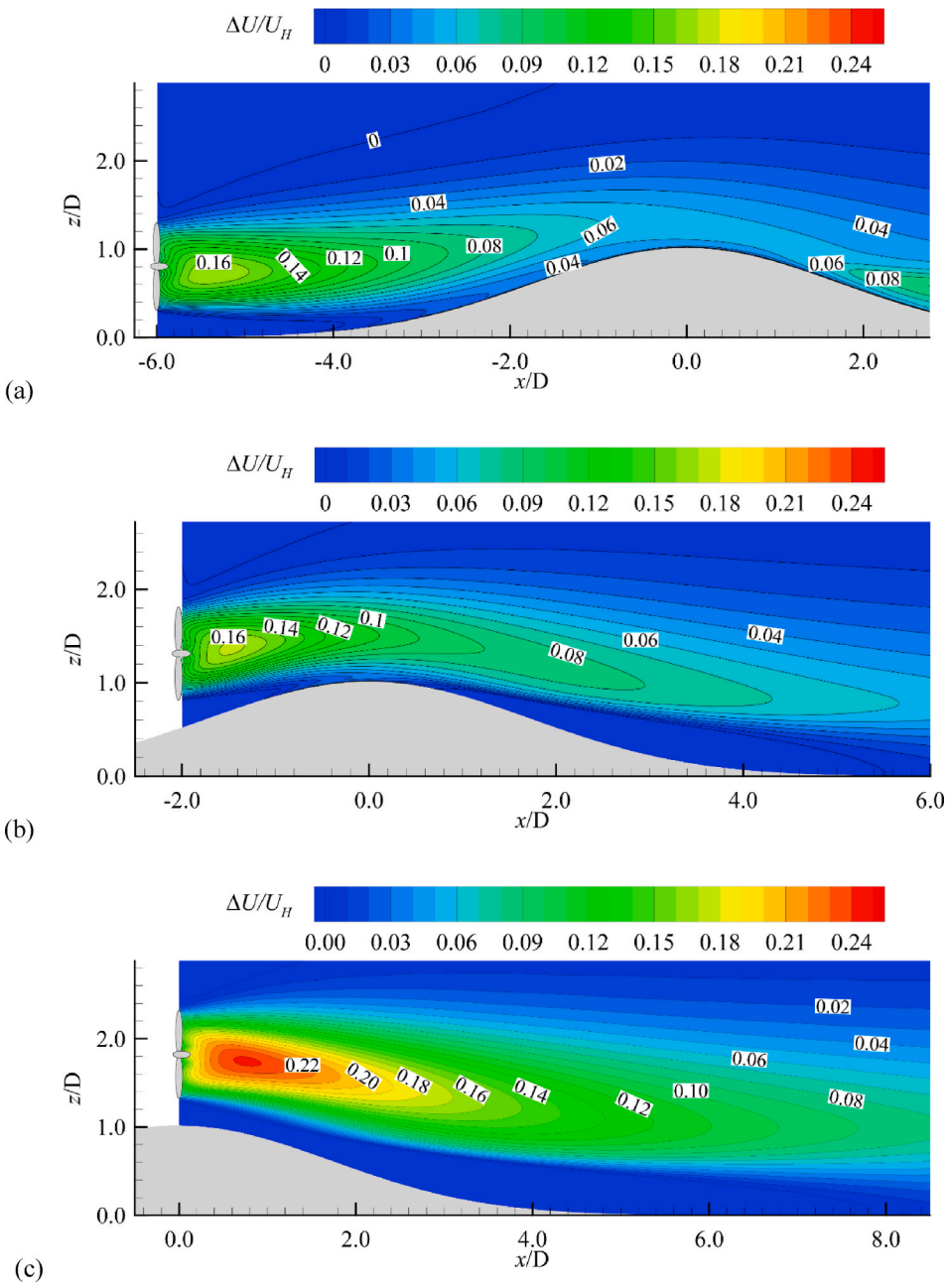

Fig. 7. Velocity deficit contours in the wake of wind turbine sited at different positions over the gentle slope hill (a) $x_{WT} = -6D$; (b)$x_{WT} = -L$; (c) $x_{WT} = 0$; (d)$x_{WT} = L$; (e) $x_{WT} = 6D$; (f) Flat terrain case.

as:

$$U_{WT,l} = S(l) \cdot U_{Flat,l} \tag{18}$$

where $S(l)$ is the speed-up factor at the location with downstream curved distance of l, and $U_{Flat,l}$ corresponds to the hub height velocity in the wake of wind turbine sited on flat terrain with downstream distance of l.

Fig. 10 shows the comparison of the velocity distributions in the wake of wind turbine sited at different locations over the hilly terrain obtained by CFD simulation and Eqn. (18). The calculations obtained using Eqn. (18) can predict the velocity distribution in the wind turbine wake with a reasonable accuracy. The maximum discrepancy appears for cases in which wind turbines are sited in front of the hilltop. As shown in Fig. 10(b), the maximum error occurs in the region near the hilltop, which is approximately 8% lower than the CFD simulation result. This is mainly caused by the fact that the acceleration of the wake recovery at the windward side of the hill is not taken into account in Eqn. (18). In addition, it can be seen in Fig. 10(c)–(e) that for the wind turbine sited on and after the hilltop, the velocity distributions predicted by Eqn. (18) are consistent with the CFD simulation results.

Compared with the Jensen wake model, the velocity in the wake of wind turbine sited on flat terrain also needs to be calculated. However, the method introduced in this study is essentially a two-step decoupled approach. Therefore, the computational costs are much lower compared with those of the fully CFD simulation of wind turbine wake propagation over complex terrain for the wind farm layout optimization.

3.2. Steep slope hilly terrain

Fig. 11 shows the velocity deficit contours caused by the wake flow

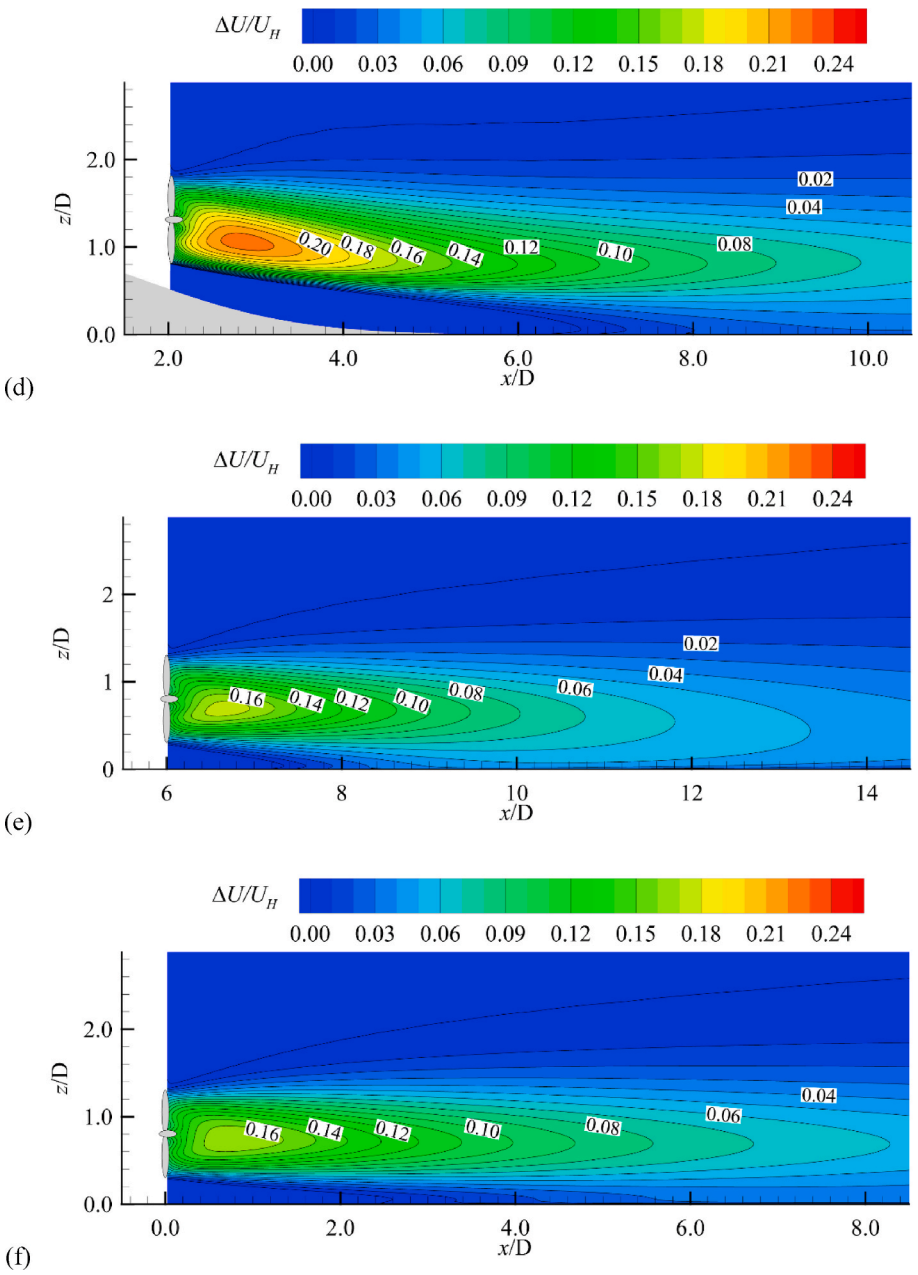

Fig. 7. (*continued*).

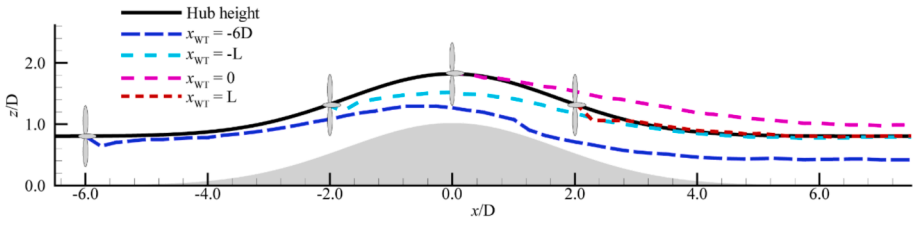

Fig. 8. Wake centerline of wind turbines sited at different locations over the gentle slope hill.

of wind turbine sited at different positions of the steep slope hill (i.e., $s = 1.0$). The centerline of the wind turbine wake is also plotted. For the wind turbine sited in front of the hill ($x_{WT} = -6D$), the flow deceleration caused by the rise in pressure in front of the hill is significant for the steep slope hill, which would restrict the recovery of wind turbine wake. The velocity deficit is relatively high in the region with wake flow approaching the hill compared with that of the gentle slope hill case. Compared with the velocity deficit, the effect of hill slope on the wake center is less obvious in the region before the hilltop. As shown in Fig. 11 (a), the height of the wake center is approximately $z' = 3/H$ on the hilltop, which is almost the same as that of the gentle slope hill case. With wake flow moving downstream of the hilltop, the propagation of

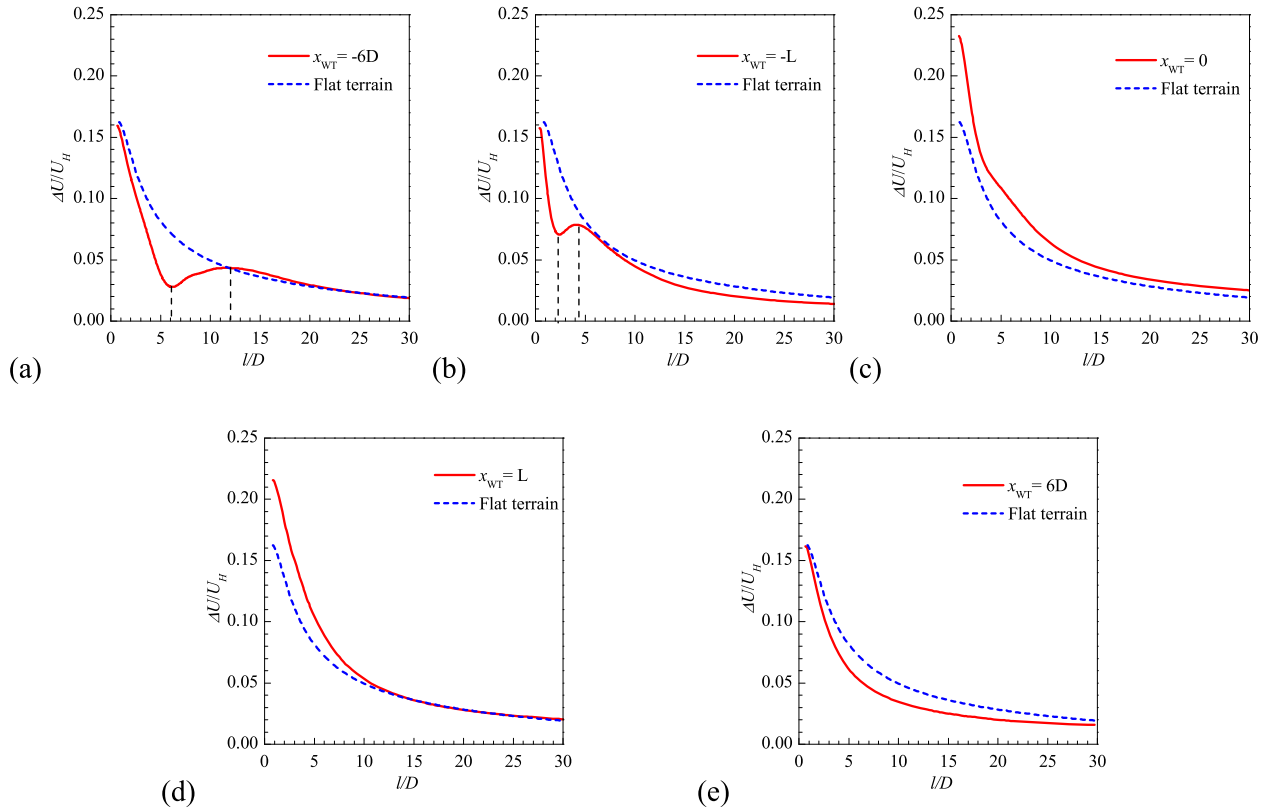

Fig. 9. Hub height velocity deficit profiles for wind turbines sited at different locations over the gentle slope hill (a) $x_{WT} = -6D$; (b)$x_{WT} = -L$; (c) $x_{WT} = 0$; (d)$x_{WT} = L$; (e).$x_{WT} = 6D$

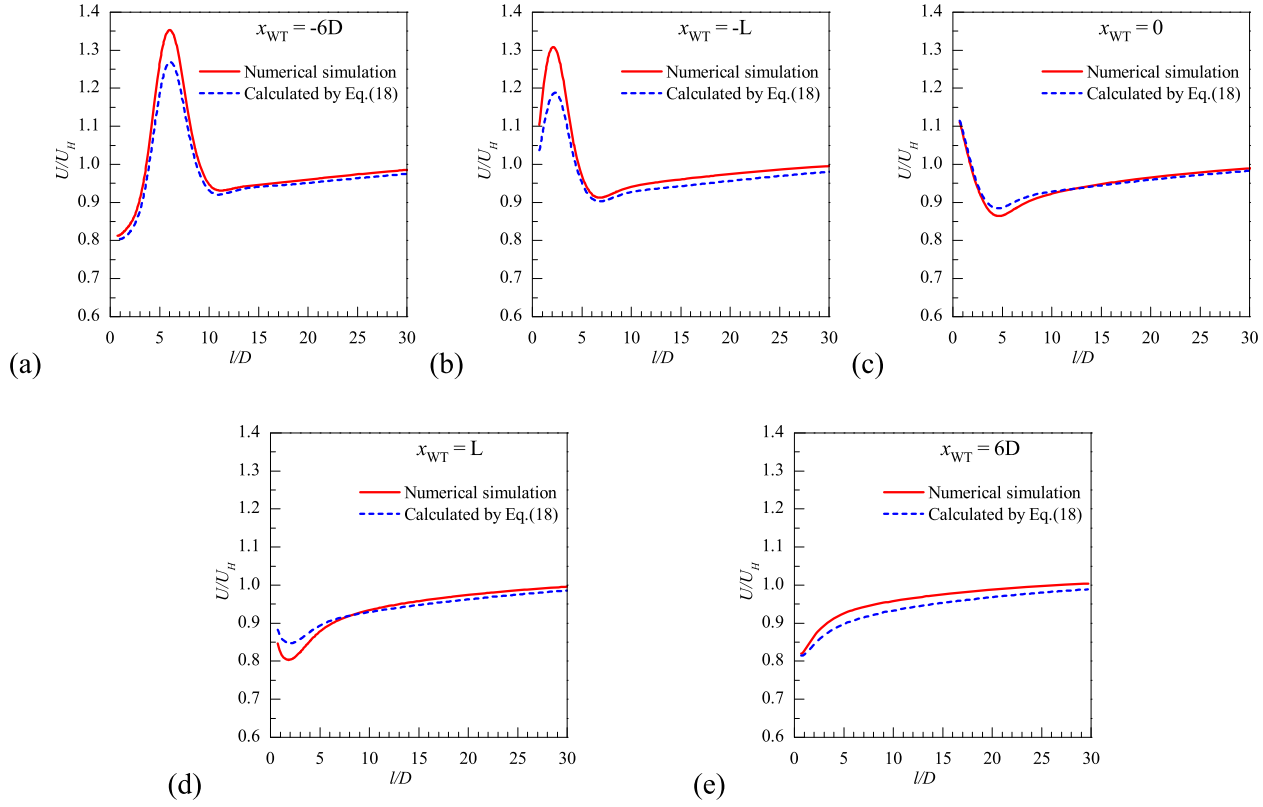

Fig. 10. Comparison of the velocity profiles in the wake of wind turbine sited at different locations over the gentle slope hill obtained by numerical simulation and Eqn. (18) (a) $x_{WT} = -6D$; (b)$x_{WT} = -L$; (c) $x_{WT} = 0$; (d)$x_{WT} = L$; (e).$x_{WT} = 6D$

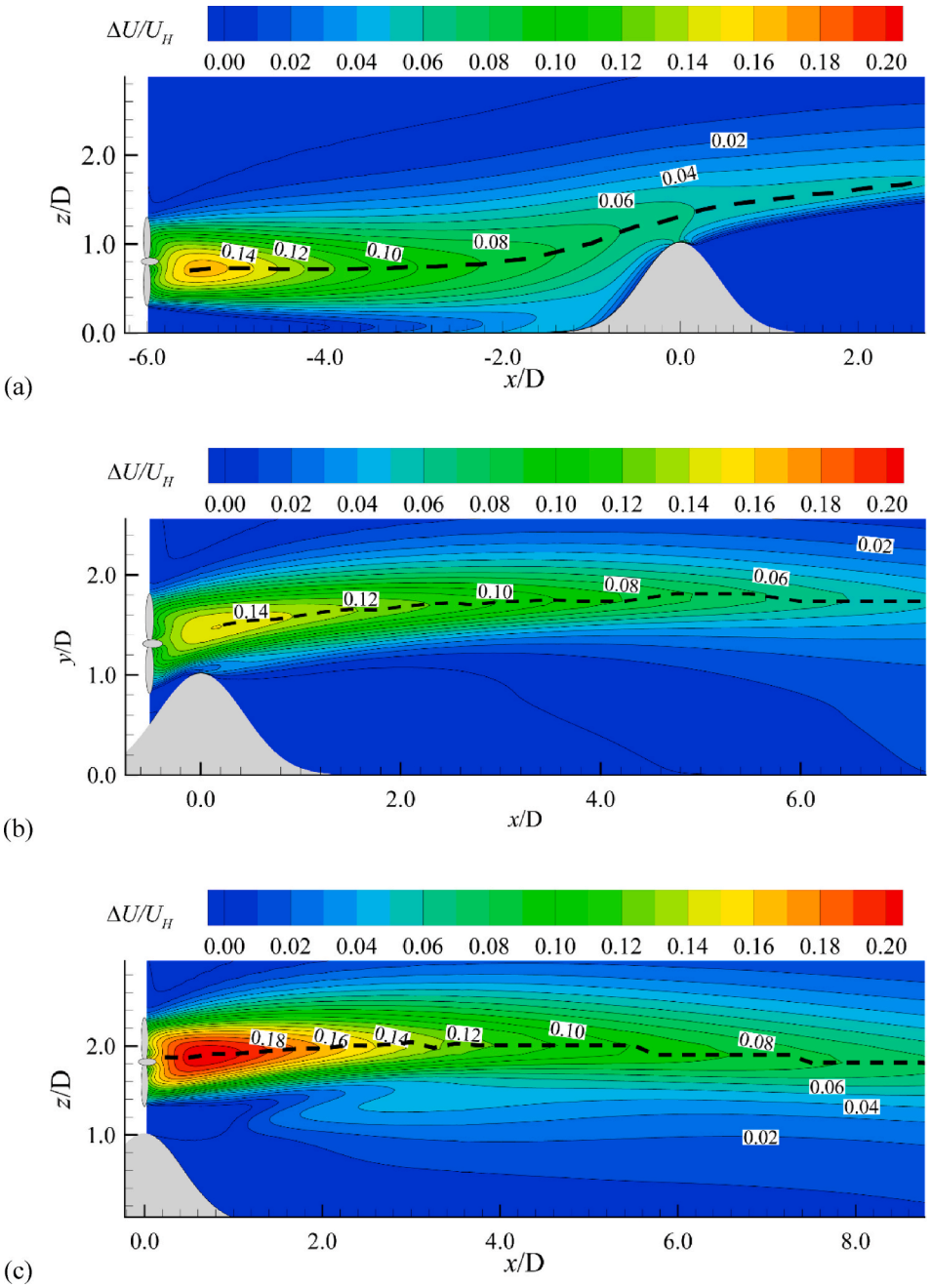

Fig. 11. Velocity deficit contours in the wake of wind turbine sited at different positions over the steep slope hill (a) $x_{WT} = -6D$; (b)$x_{WT} = -L$; (c).$x_{WT} = 0$

wind turbine wake significantly deviated from that of the gentle slope hill case. The flow upwash caused by the increase in hill height at the windward side of the hill remains in the region behind the hilltop. As shown in Fig. 11(a), the wake center height continues to increase for a long distance downstream of the hilltop. Compared with the gentle slope hill case, this significant change in the wake center can be attributed to the large flow separation at the lee side of the hill, which prevents the wake flow from moving toward the ground.

With the wind turbine sited at the windward side of the hill ($x_{WT} = -L$), the speed-up effect is more evident for the steep slope hill because of the sharp increase in hill height. Figs. 7(b) and Figure 11(b) show that the recovery of wind turbine wake is faster for the steep slope hill case. Behind the hilltop, the wake center height continues to increase for a long downstream distance ($x = 5D$) and then gradually decreases with the wake flow moving further downstream. The change in hill height has almost no effect on the wake center height. A similar phenomenon can be observed with the wind turbine sited on the hilltop, as shown in Fig. 11(c). For wind turbines sited over hilly terrain with a steep slope, no correlation was observed between the wake centerline and the hill shape in the region behind the hilltop. The assumption that the wake centerline follows the surface of the hill is no longer applicable. Therefore, this engineering wake model could result in significant errors for the wind farm layout optimization over steep slope complex terrain.

The velocity deficits along the wake centerline with wind turbine sited at different locations over the steep and gentle slope hill cases are plotted in Fig. 12. For the wind turbine sited in front of the hilltop ($x_{WT} = -6D, -L$), the two turning points for the gentle slope hill case disappear. It can be seen in Fig. 12(a)–(b) that the velocity deficit for the steep slope hill case continues to decrease as the downstream distance increases.

In the region behind the hilltop, the flow separation at the lee side of the hill prevents the wake flow from moving toward the ground. The

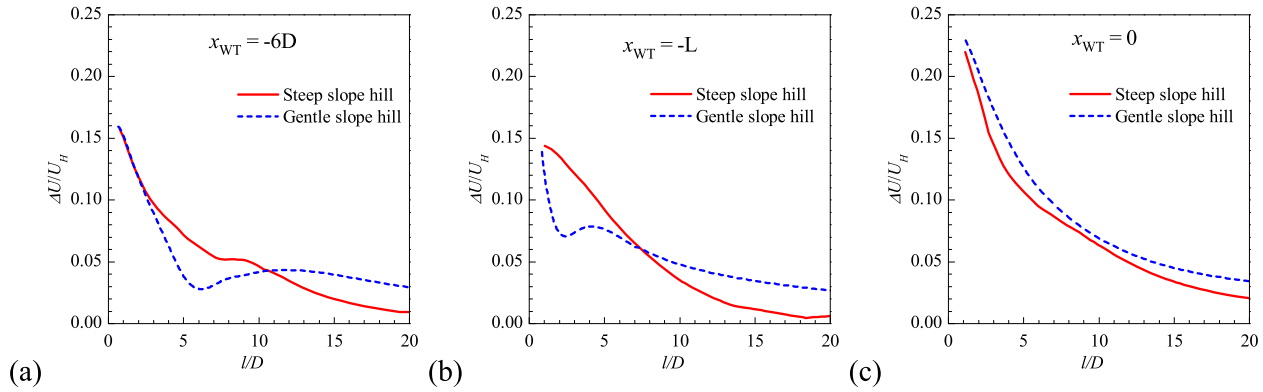

Fig. 12. Velocity deficits along the wake centerline with wind turbine sited at different locations over the steep and gentle slope hills (a) $x_{WT} = -6D$; (b)$x_{WT} = -L$; (c).$x_{WT} = 0$

expansion of wind turbine wake is also highly restricted by the separation flow. Therefore, as shown in Figs. 7 and 11, the altitude of the wake zone is much higher for the steep slope hill case in the region behind the hilltop. Compared with the gentle slope hill, the wind turbine wake at higher altitude can be mixed with higher speed outer ABL wind, thereby accelerating the recovery of the wind turbine wake. Therefore, it can be seen in Fig. 12 that the wake recovery in the far wake region is always faster for the steep slope hill case compared with the gentle slope hill case for all three tested cases.

Fig. 13 shows the influence of wind turbine wake on the flow separation zone at the lee side of the hill. For wind turbine located 6*D* in front of the hilltop ($x_{WT} = -6D$), the wind turbine wake has a long distance to mix with the surrounding flow, thereby increasing the turbulent kinetic energy (TKE) of the downstream flow. This enhanced TKE in the flow would make the separation point move backward and reduce the separation zone at the lee side of the hill. A similar flow feature was also reported by Taylor et al. (1991). However, for the wind turbine located near the hilltop (i.e., $x_{WT} = -L$ and 0), there is not enough distance for the turbulence mixing of the wind turbine wake and the surrounding ABL wind. Therefore, as shown in Fig. 13, the wake flow has no obvious effect on the flow separation zone.

It should be noted that the topographies simulated in the present study are uniformly shaped two-dimensional hills. Gong and Ibbetson (1989) compared the turbulent flow over two- and three-dimensional hills. They indicated that for a gentle hill, a reduced perturbation amplitude can be obtained for three-dimensional hill. The speed-up effect at the windward side and the strength of wake flow at the lee side would be reduced for the three-dimensional hill compared with those for the two-dimensional hill of similar cross-section. Furthermore, Politis et al. (2012) compared the velocity deficit caused by wind turbine sited on the top of two- and three-dimensional hills. They found that the recovery of wind turbine wake at the lee side of the three-dimensional hill is faster than that of the two-dimensional hill case. Ishihara et al. (1999) experimentally studied the turbulent flow over a three-dimensional steep hill. It was found that the pronounced speed-up of flow occurs not only on the hilltop but also at the midway of the sides. Meanwhile, the ABL wind over a three-dimensional steep hill separates behind the crest and reattaches just at the lee foot of the hill, which is different from that of the two-dimensional hill.

In addition, terrain roughness is also an important factor to influence the flow characteristics over the hilly terrain and the propagation of wind turbine wake. Cao and Tamura (2006) indicated that the surface roughness increases the speed-up ratio above the crest. Later, they (Cao and Tamura, 2007) studied the effects of sudden changes in roughness on the turbulent flow over a steep hill, and found that adding or removing roughness blocks on the hill surface or inflow area changes the velocity deficit and creates a completely different turbulence structure in the wake. Barlas et al. (2016) indicated that the terrain roughness would increase the turbulence level of incoming flow, resulting in an enhanced mixing between the wind turbine wake and the surrounding high momentum flow. Meanwhile, the axisymmetric structure of wind turbine wakes would be broken by the incoming ABL wind. According to Chamorro and Porté-Agel (2009), this trend would be more evident with increasing surface roughness due to the increased inhomogeneity of velocity and turbulence levels.

4. Conclusions

In this study, a RANS simulation combined with actuator disk model was conducted to quantify the wake characteristics of wind turbines sited at different locations over two-dimensional Gaussian hills. The effect of topography on the wake characteristics such as velocity deficit, wake expansion and wake center movement was systematically analyzed and compared with the Jensen wake model for the optimal design of the wind turbine layout over complex terrain.

The velocity deficit in the wind turbine wake is highly affected by the topography for the gentle slope hill. For the wind turbine sited in front of the hilltop, the velocity deficit does not monotonously decrease with the downstream distance. An increase in velocity deficit is observed within a certain distance behind the hilltop. For the wind turbine sited on the hilltop and over the downgrade of the hill, the velocity deficit in the wind turbine wake can be significantly enhanced by the adverse pressure gradient at the lee side of the hill. However, only the speed-up factor at the wind turbine location is adopted in the Jensen wake

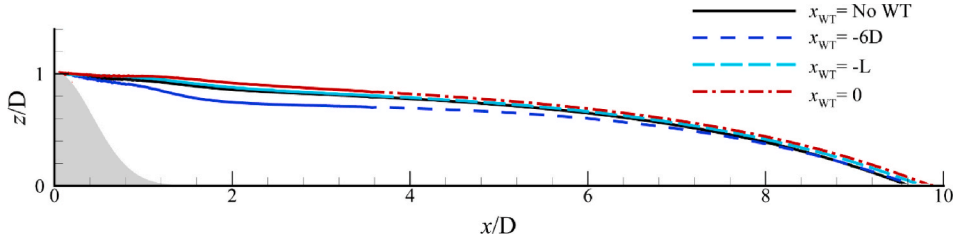

Fig. 13. Comparison of the flow separation region at the lee side of the steep slope hill.

model. The effects of downstream topography on the wind turbine wake mentioned above are not taken into consideration. In this study, a new method is proposed based on the local speed-up factor and the simulated velocity in the wake of wind turbine sited on flat terrain, which can more reasonably predict the velocity variation along the centerline of the wind turbine wake over complex terrain.

In the current engineering wake model, the centerline of wind turbine wake is generally assumed to follow the surface of the hill with the wake center height equaling to the wind turbine hub height *H*. However, this assumption is only reasonable for wind turbine wake in the region with a gentle change in hill height. In the region with a sharp change in hill height, the change in the wake center shows an obvious delay compared with the change in hill height.

For the steep slope hill, the propagation in wind turbine wake in the region behind the hilltop significantly differs from that of the gentle slope hill case. There is no correlation between the wake centerline and the hill shape in the region behind the hilltop. The assumption that the wake centerline follows the surface of the hill is no longer applicable. Compared with the gentle slope hill, the recovery of wind turbine wake in the far wake region was found to always be faster for the steep slope hill case. This acceleration of wake recovery is believed to be closely related to the large separation flow at the lee side of the hill, which highly restricts the downward deflection and expansion of the wind turbine wake.

It should be noted that the current simulation of wind turbine wake over hilly terrain is conducted under neutral condition. Zhang et al. (2012) experimentally compared the wake characteristics of wind turbine sited in a convective boundary layer (CBL) and a neutral boundary layer. They indicated that in comparison with the wake of the same wind turbine in a neutral boundary layer, a smaller velocity deficit (about 15% at the wake center) can be observed in the CBL. Meanwhile, the magnitude of peak turbulence intensity in the wake is approximately 20% higher in the CBL than that in the neutral boundary layer. El-Askary et al. (2017) numerically studied the wind turbine wakes under thermally-stratified atmospheric boundary layer, and found that there is a significant influence of the different atmospheric conditions on the wake behavior. The wake region was found to become smaller with the decreasing of atmospheric stability. In addition, Menke et al. (2018) has demonstrated that whether the wind turbine wake follows the terrain strongly depends on the thermal stability conditions and the terrain orography. Therefore, a detailed investigation is still needed to fully explore the thermal effects on the wake characteristics of wind turbines sited over complex terrain.

CRediT authorship contribution statement

Wei Tian: Conceptualization, Methodology, Formal analysis, Writing – original draft, Funding acquisition, Supervision. **Kuan Zheng:** Data acquisition and processing, Formal analysis. **Hui Hu:** Conceptualization, Writing – review & editing, Supervision.

Declaration of competing interest

The authors declare that they have no known competing financial interests or personal relationships that could have appeared to influence the work reported in this paper.

Acknowledgement

Funding supports from National Natural Science Foundation of China (No. 11872039) and Natural Science Foundation of Shanghai (No.16ZR1417600) are gratefully acknowledged.

References

Astolfi, D., Castellani, F., Terzi, L., 2018. A study of wind turbine wakes in complex terrain through RANS simulation and SCADA data. J. Sol. Energ. 140 (3), 031001.
Barlas, E., Buckingham, S., van Beeck, J., 2016. Roughness effects on wind-turbine wake dynamics in a boundary-layer wind tunnel. Boundary-Layer Meteorol. 158 (1), 27–42.
Barthelmie, R.J., Frandsen, S.T., Nielsen, M.N., 2007. Pryor S C, Rethore P E, Jørgensen H E. Modelling and measurements of power losses and turbulence intensity in wind turbine wakes at Middelgrunden offshore wind farm. Wind Energy 10, 517–528.
Barthelmie, R.J., Larsen, G.C., Frandsen, S.T., Folkerts, L., Rados, K., Pryor, S.C., Lange, B., Schepers, G., 2006. Comparison of wake model simulations with offshore wind turbine wake profiles measured by sodar. J. Atmos. Ocean. 23 (7), 888–901.
Behrouzifar, A., Darbandi, M., 2019. An improved actuator disc model for the numerical prediction of the far-wake region of a horizontal axis wind turbine and its performance. Energy Convers. Manag. 185, 482–495.
Berg, J., Troldborg, N., Sørensen, N.N., Patton, E.G., Sullivan, P.P., 2017. Large-eddy simulation of turbine wake in complex terrain. J. Phys. Conf. Ser. 854 (1), 012003.
Blocken, B., Stathopoulos, T., Carmeliet, J., 2007. CFD simulation of the atmospheric boundary layer: wall function problems. Atmos. Environ. 41 (2), 238–252.
Cao, S., Tamura, T., 2006. Experimental study on roughness effects on turbulent boundary layer flow over a two-dimensional steep hill. J. Wind Eng. Ind. Aerod. 94, 1–19.
Cao, S., Tamura, T., 2007. Effects of roughness blocks on atmospheric boundary layer flow over a two-dimensional low hill with/without sudden roughness change. J. Wind Eng. Ind. Aerod. 95, 679–695.
Chamorro, L.P., Porté-Agel, F., 2009. A wind tunnel investigation of wind turbine wakes: boundary-layer turbulence effects, Bound. Layer Meteorol 132, 129–149.
Cheng, W.C., Fernando, P.A., 2018. A simple physically-based model for wind-turbine wake growth in a turbulent boundary layer. Bound.-Layer Meteorol. 169, 1–10.
Chu, C.R., Chiang, P.H., 2014. Turbulence effects on the wake flow and power production of a horizontal-axis wind turbine. J. Wind Eng. Ind. Aerod. 124, 82–89.
El-Asha, S., Zhan, L., Iungo, G.V., 2017. Quantification of power losses due to wind turbine wake interactions through SCADA, meteorological and wind LiDAR data. Wind Energy 20, 1823–1839.
El-Askary, W.A., Sakr, I.M., AbdelSalam, A.M., Abuhegazy, M.R., 2017. Modeling of wind turbine wakes under thermally-stratified atmospheric boundary layer. J. Wind Eng. Ind. Aerod. 160, 1–15.
Feng, J., Shen, W.Z., 2014. Wind farm layout optimization in complex terrain: a preliminary study on a Gaussian hill. J. Phys. Conf. Ser. 524, 1–11.
Frandsen, S., 1992. On the wind speed reduction in the center of large clusters of wind turbines. J. Wind Eng. Ind. Aerod. 39, 251–265.
Garcia, E.T., Aubrun, S., Coupiac, O., Girard, N., Boquet, M., 2018. Statistical characteristics of interacting wind turbine wakes from a 7-month LiDAR measurement campaign. Renew. Energy 130, 1–11.
Ge, M., Wu, Y., Liu, Y., Li, Q., 2019a. A two-dimensional model based on the expansion of physical wake boundary for wind-turbine wakes. Appl. Energy 233–234, 975–984.
Ge, M., Wu, Y., Liu, Y., Yang, X., 2019b. A two-dimensional Jensen model with a Gaussian-shaped velocity deficit. Renew. Energy 141 (10), 46–56.
Göçmen, T., van der Laan, P., Réthoré, P.E., Diaz, A.P., Larsen, G.C., Ott, S., 2016. Wind turbine wake models developed at the technical university of Denmark: a review. Renew. Sustain. Energy Rev. 60, 752–769.
Gong, W., Ibbetson, A., 1989. A wind tunnel study of turbulent flow over model hills. Bound. Layer Meteorol 49, 113–148.
Hansen, K., Larsen, G., Menke, R., Vasiljevic, N., Angelou, N., Feng, J., 2016. Wind turbine wake measurement in complex terrain. J. Phys. Conf. Ser. 753 (3), 032013.
Howard, K.B., Hu, J.S., Chamorro, L.P., Guala, M., 2015. Characterizing the response of a wind turbine model under complex inflow conditions. Wind Energy 18 (4), 729–743.
Hu, H., Yang, Z., Sarkar, P., 2012. Dynamic wind loadings and wake characteristics of a wind turbine model in an atmospheric boundary layer wind. Exp. Fluid 52, 1277–1294.
Hyvärinen, A., Lacagnina, G., Segalini, A., 2018. A wind-tunnel study of the wake development behind wind turbines over sinusoidal hills. Wind Energy 21 (8), 605–617.
Ibrahim, O.M., Yoshida, S., Hamasaki, M., Takada, A., 2019. Wind turbine wake modeling in accelerating wind field: a preliminary study on a two-dimensional hill. Fluid 4 (3), 153.
Ishihara, T., Hibi, K., Oikawa, S., 1999. A wind tunnel study of turbulent flow over a three-dimensional steep hill. J. Wind Eng. Ind. Aerod. 83, 95–107.
Jensen, N.O., 1983. A Note on Wind Generator Interaction. Technical Report Risø-M-2411, Risø.
Keane, A., 2021. Advancement of an analytical double-Gaussian full wind turbine wake model. Renew. Energy 171, 687–708.
Kim, H.G., Patel, V.C., Lee, C.M., 2000. Numerical simulation of wind flow over hilly terrain. J. Wind Eng. Ind. Aerod. 87, 45–60.
Kuo, J.Y.J., Romero, D.A., Beck, J.C., Amon, C.H., 2016. Wind farm layout optimization on complex terrains-Integrating a CFD wake model with mixed-integer programming. Appl. Energy 178, 404–414.
Lange, J., Mann, J., Berg, J., Dan, P., Hangan, H., 2017. For wind turbines in complex terrain, the devil is in the detail. Environ. Res. Lett. 12 (9), 094020.
Makridis, A., Chick, J., 2013. Validation of a CFD model of wind turbine wakes with terrain effects. J. Wind Eng. Ind. Aerod. 123, 12–29.
Menke, R., Vasiljević, N., Hansen, K.S., Hahmann, A.N., Mann, J., 2018. Does the wind turbine wake follow the topography? A multi-lidar study in complex terrain. Wind Energy Science 3 (2), 681–691.

Mikkelsen, R., 2004. Actuator Disc Methods Applied to Wind Turbines. PhD dissertation. Department of Mechanical Engineering. Technical University of Denmark, Lyngby.
Nedjari, H.D., Guerri, O., Saighi, M., 2017. CFD wind turbines wake assessment in complex topography. Energy Convers. Manag. 138, 224–236.
Politis, E.S., Prospathopoulos, J., Cabezon, D., Hansen, K.S., Chaviaropoulos, P.K., Barthelmie, R.J., 2012. Modeling wake effects in large wind farms in complex terrain the problem, the methods and the issues. Wind Energy 15, 161–182.
Prospathopoulos, J.M., Politis, E.S., Chaviaropoulos, P.K., 2008. Modelling Wind Turbines in Complex Terrain. European Wind Energy Conference, Brussels, Belgium.
Schreck, S., Lundquist, J., Shaw, W., 2008. U. S. Department of Energy Workshop Report: Research Needs for Wind Resource Characterization. National Renewable Energy Laboratory technical report, NREL/TP-500-43521.
Shamsoddin, S., Porté-Agel, F., 2018. Wind turbine wakes over hills. J. Fluid Mech. 855, 671–702.
Shayan, N., Sogand, P., Farschad, T., 2018. Modeling of horizontal axis wind turbine wakes in Horns Rev offshore wind farm using an improved actuator disc model coupled with computational fluid dynamic. Energy Convers. Manag. 171, 953–968.
Shen, W.Z., Zhu, W.J., Barlas, E., Li, Y., 2019. Advanced flow and noise simulation method for wind farm assessment in complex terrain. Renew. Energy 143, 1812–1825.
Song, M.X., Chen, K., He, Z.Y., Zhang, X., 2012. Wake flow model of wind turbine using particle simulation. Renew. Energy 41, 185–190.
Taylor, G.J., Smith, D., 1991. Wake measurements over complex terrain. In: Proceedings of the 13th BWEA Wind Energy Conference, pp. 335–342. Swansea, UK.
Thomsen, K., Soerensen, P., 1999. Fatigue loads for wind turbines operating in wakes. J. Wind Eng. Ind. Aerod. 80 (1), 121–136.
Tian, L., Zhu, W., Shen, W., Zhao, N., Shen, Z., 2015. Development and validation of a new two-dimensional wake model for wind turbine wakes. J. Wind Eng. Ind. Aerod. 137, 90–99.
Tian, W., Ozbay, A., Hu, H., 2014. Effects of incoming surface wind conditions on the wake characteristics and dynamic wind loadings acting on a wind turbine model. Phys. Fluids 26, 125108.
Tian, W., Ozbay, A., Hu, H., 2018. An experimental investigation on the aeromechanics and wake interferences of wind turbines sited over complex terrain. J. Wind Eng. Ind. Aerod. 172, 379–394.
Wu, Y.T., Porté-Agel, F., 2011. Large-eddy simulation of wind-turbine wakes: evaluation of turbine parametrisations. Bound.-Layer Meteorol. 138 (3), 345–366.
Yang, X., Howard, K.B., Guala, M., Sotiropoulos, F., 2015. Effects of a Three-dimensional hill on the wake characteristics of a model wind turbine. Phys. Fluids 27 (2), 025103.
Yang, Y., Gu, M., Chen, S., Jin, X., 2009. New inflow boundary conditions for modelling the neutral equilibrium atmospheric boundary layer in computational wind engineering. J. Wind Eng. Ind. Aerod. 97 (2), 88–95.
Zhan, L., Letizia, S., Iungo, G.V., 2020. LiDAR measurements for an onshore wind farm: wake variability for different incoming wind speeds and atmospheric stability regimes. Wind Energy 23 (3), 501–527.
Zhang, W., Markfort, C.D., Porté-Agel, F., 2012. Wind-turbine wakes in a convective boundary layer: a wind-tunnel study. Bound.-Layer Meteorol. 146 (2), 161–179.